

An oceanographic three-dimensional variational data assimilation scheme

Srdjan Dobricic^{a,*}, Nadia Pinardi^b

^a *Centro Euro-Mediterraneo per i Cambiamenti Climatici, Via Aldo Moro 44, 40139 Bologna, Italy*

^b *Corso di Scienze Ambientali, University of Bologna, Ravenna, Italy*

Received 22 August 2007; received in revised form 21 January 2008; accepted 21 January 2008

Available online 2 February 2008

Abstract

This study describes the development and evaluation of an oceanographic three-dimensional variational (3D-VAR) data assimilation scheme based on a novel specification of the background error covariances. The new 3D-VAR scheme allows for regional variability of the background error covariance matrix, complex coastal boundary conditions and variable bottom topography. The error covariance matrix is formed by the successive application of linear operators that can consider vertical EOFs, horizontal covariance functions that consider coastlines, sea level corrections that vary from shallow to deep regions and divergence dumping of velocity corrections near the coasts. The scheme is applied to the Mediterranean Sea and the quality of analysis is assessed by comparing background estimates with observations in the period October 2005–October 2006.

© 2008 Elsevier Ltd. All rights reserved.

Keywords: Data assimilation; Operational oceanography; Ocean models

1. Introduction

Since 1999, the Mediterranean forecasting system (MFS) has been operationally producing analyses in the Mediterranean Sea (Pinardi et al., 2003). It uses an optimal interpolation scheme, the so-called SOFA (De Mey and Benkiran, 2002), to assimilate Sea level anomaly (SLA) observed by satellites (Le Traon et al., 2003), temperature and salinity profiles from XBT (Manzella et al., 2007) and Argo floats (Poulain et al., 2007). A specific feature of SOFA is the separation of the background error covariance matrix into vertical and horizontal modes. Horizontal covariances are modelled as Gaussian functions, whilst vertical error covariances are represented by Empirical Orthogonal Functions (EOFs), calculated from the variance of a long-term model simulation (e.g. Dobricic et al., 2005). In practice, only the most significant EOFs

are used, and the number of EOFs is much smaller than the size of the control vector in the physical space. In this way the size of the background error covariance matrix is significantly reduced. As it is never stored in the memory of the computer, but calculated locally at each model point, the size reduction by EOFs reduces the computational effort needed to calculate and invert locally the background error covariance matrix. Another advantage of the reduced order representation by EOFs is that the background error covariances are efficiently filtered by eliminating statistically insignificant covariances.

Demirov et al. (2003) made the initial set-up of the scheme in the Mediterranean. The application of seasonally and regionally varying EOFs with SOFA is described in Dobricic et al. (2005), whilst Dobricic et al. (2007) describe the daily assimilation cycle, the impact of the assimilation of in situ temperature and salinity observations, the impact of the geostrophic balance enforcement on the EOFs and the impact of the velocity corrections on the analyses. The relatively long-term operational application of SOFA

* Corresponding author. Tel.: +39 0 513782637.
E-mail address: dobricic@bo.ingv.it (S. Dobricic).

in the Mediterranean showed that the quality of the analyses was very sensitive to the specification the background error covariance matrix, which now has regional and seasonal variability. However, probably the most important factor which influenced the quality of the analyses was the number of assimilated observations and the number of model variables which were directly observed (Dobricic et al., 2007). The use of an optimal interpolation scheme requires a relatively complex implementation of the linearized observational operator, because the Kalman gain contains this operator several times, multiplying the background error covariance matrix. It may therefore become difficult with SOFA to assimilate observations with complicated observational operators or make the existing observational operators more complex. Another disadvantage of optimal interpolation is that the solution is always local and discontinuities might appear in the analysis due to the presence of nearby observations (e.g. Gauthier et al., 1999) or discontinuous regional EOFs (Bellucci et al., 2008). The negative impact of the local operator on the analysis field may be attenuated by the usage of overlapping observations and EOFs. However, in this way the problem is alleviated by arbitrary assumptions involving an additional computational cost. Furthermore, the computational cost of an optimal interpolation scheme is approximately proportional to the number of observations that are assimilated. In the future this cost may become unaffordable since the number of available satellite and in situ observations is rapidly growing and may continue to grow faster than the available computer power in coming years. On the other hand, the computational cost of a 3D-VAR scheme mainly depends on the size of the model state vector and much less on the number of observations. Therefore, we may expect that the application of the 3D-VAR may facilitate the use of a relatively large number of observations which were not used previously with SOFA. In this way it could significantly improve the quality of the analyses and forecasts of the MFS.

Variational schemes have been applied in meteorology for a relatively long time, showing an improvement in the analysis quality in comparison to optimal interpolation schemes (e.g. Rabier, 2005). On the other hand, most operational systems in oceanography currently use optimal interpolation schemes (e.g. Dobricic et al., 2005), the SEEK filter or the Ensemble Kalman Filter (Brasseur et al., 2005) but not variational schemes. These last have been mainly used in oceanographic re-analyses with relatively coarse resolution models (e.g. Derber and Rosati, 1989; Masina et al., 2001; Stammer et al., 2002; Weaver et al., 2003; Fujii and Kamachi, 2003; Weaver et al., 2005).

This paper describes the development and application of a new oceanographic 3D-VAR assimilation scheme. Its implementation in operational systems requires several novel practical solutions, which have to be computationally efficient and sufficiently accurate, in order to account for specific oceanographic issues, like the coastlines and variable bottom topography, as well as dynamically

adjusted corrections. Section 2 gives a general description of the 3D-VAR scheme and explains the numerical method used for the minimization of the cost function. Section 3 describes the background error covariance matrix definitions. In Section 4, we show the implementation of the 3D-VAR in the Mediterranean Sea and its impact on the accuracy of ocean state estimates. Section 4 gives the conclusions.

2. General description

2.1. Cost function formalism

The 3D-VAR scheme iteratively finds the minimum of the following cost function:

$$J = \frac{1}{2}(\mathbf{x} - \mathbf{x}_b)^T \mathbf{B}^{-1}(\mathbf{x} - \mathbf{x}_b) + \frac{1}{2}(H(\mathbf{x}) - \mathbf{y})^T \mathbf{R}^{-1}(H(\mathbf{x}) - \mathbf{y}), \quad (1)$$

where \mathbf{x} is the analysis state vector, \mathbf{x}_b is the background state vector, \mathbf{B} is the background error covariance matrix, \mathbf{R} is the observational error covariance matrix and H is the non-linear observational operator. Eq. (1) is linearized around the background state (e.g. Lorenc, 1997) into the following form:

$$J = \frac{1}{2}\delta\mathbf{x}^T \mathbf{B}^{-1}\delta\mathbf{x} + \frac{1}{2}(\mathbf{H}\delta\mathbf{x} - \mathbf{d})^T \mathbf{R}^{-1}(\mathbf{H}\delta\mathbf{x} - \mathbf{d}), \quad (2)$$

where $\mathbf{d} = [\mathbf{y} - H(\mathbf{x}_b)]$ is the misfit, \mathbf{H} is the linearized observational operator evaluated at $\mathbf{x} = \mathbf{x}_b$ and $\delta\mathbf{x} = \mathbf{x} - \mathbf{x}_b$ are the increments. The state vector considered in our study contains the following model state variables:

$$\mathbf{x} = [T, S, \eta, u, v]^T, \quad (3)$$

where T is the three-dimensional temperature field, S the three-dimensional salinity field, η the two-dimensional free surface elevation, and u, v are the total horizontal velocity components. In Eq. (2) the minimization problem is defined on the field of increments. The linearization creates a quadratic cost function which has a single minimum. In order to avoid the inversion of \mathbf{B} and to precondition the minimization of the cost function it is assumed that \mathbf{B} can be written in the form:

$$\mathbf{B} = \mathbf{V}\mathbf{V}^T, \quad (4)$$

and the cost function is minimized using a new control variable \mathbf{v} (e.g. Lorenc, 1997) defined using the transformation matrix \mathbf{V}^+ :

$$\mathbf{v} = \mathbf{V}^+ \delta\mathbf{x}, \quad (5)$$

where the superscript “+” indicates the generalized inverse. The vector \mathbf{v} is defined on the control space, and the vector $\delta\mathbf{x}$ on the physical space. The cost function (2) now has the form:

$$J = \frac{1}{2}\mathbf{v}^T \mathbf{v} + \frac{1}{2}(\mathbf{H}\mathbf{V}\mathbf{v} - \mathbf{d})^T \mathbf{R}^{-1}(\mathbf{H}\mathbf{V}\mathbf{v} - \mathbf{d}). \quad (6)$$

2.2. Background error covariance matrix

Due to its large size, the transformation matrix \mathbf{V} is modelled at each minimization iteration as a sequence of linear operators (e.g. Weaver et al., 2003). In this way \mathbf{V} successively transforms increments in the control space towards final increments in the physical space. Considering specific requirements for oceanographic problems, the matrix \mathbf{V} is defined in the following way:

$$\mathbf{V} = \mathbf{V}_D \mathbf{V}_{uv} \mathbf{V}_\eta \mathbf{V}_H \mathbf{V}_V. \quad (7)$$

In Eq. (7) the linear operator \mathbf{V}_V transforms coefficients which multiply vertical EOFs into vertical profiles of temperature and salinity defined at the model vertical levels, \mathbf{V}_H applies horizontal covariances on fields of temperature and salinity, \mathbf{V}_η calculates the sea surface height error covariance from three dimensional fields of temperature and salinity, \mathbf{V}_{uv} calculates velocity from sea surface height, temperature and salinity, and \mathbf{V}_D applies a divergence damping filter on the velocity field. The formulation of each linear operator is described in Section 3.

2.3. Numerical minimization

Most of the computational time necessary to minimize the 3D-VAR cost function is spent in the transformation of increments from the control space to the physical space by the linear operator \mathbf{V} and its transpose. Therefore, the computational cost of the 3D-VAR is approximately proportional to the size of the control vector \mathbf{v} . Furthermore, it also depends on the complexity of linear operators used in Eq. (7). It is important to note that the reduction in computational time obtained by using vertical EOFs in the 3D-VAR is larger than in the optimal interpolation scheme. In addition to reducing the number of operations on the state vector inside the minimizer code, the use of EOFs in the 3D-VAR reduces the size of the control vector \mathbf{v} and therefore may reduce the number of iterations of the minimizer (e.g. Robert et al., 2005).

To increase further the computational efficiency of the scheme, we have applied a multigrid approach. The multigrid method is well known for the solution of partial differential equations (Brandt, 1977; Briggs et al., 2000). In the data assimilation this approach has been implemented in spectral space by Courtier et al. (1994). As our model is defined on grid points, our multigrid approach first computes the analysis on a grid with a lower spatial resolution, and then interpolates this solution to a finer grid for the further minimization. This is implemented in the 3D-VAR algorithm by an outer loop over the different grids, and an inner loop that minimizes the cost function on each grid. An additional advantage of the multigrid approach is that, if we assume that the interpolated analysis is already sufficiently accurate, we do not even have to perform further minimizations on the finer resolution grid (Courtier et al., 1994). Another way to reduce the computational load is to apply a simplified version of linear operators in (7) dur-

ing the first iterations of the outer loop, and then use that solution as a first guess for the minimization in the next iteration with the full linear operators (Courtier et al., 1994). As when the grids have different resolutions, this method is applied in the outer loop of the 3D-VAR with computationally expensive operators \mathbf{V}_η and \mathbf{V}_D (see Section 3).

The cost function is numerically minimized using the quasi-Newton L-BFGS minimizer (Byrd et al., 1995). Iterations of the minimizer are stopped when the absolute value of the gradient of the cost function becomes small relative to its initial value (typically one percent of the initial value). The calculation of the gradient of the cost function requires the adjoint of the operators \mathbf{V} and \mathbf{H} . The adjoint is formulated by hand-coding the transpose of each subroutine containing operators \mathbf{V} and \mathbf{H} , following rules given by Giering and Kaminski (1998).

3. Background error covariance modelling by linear operators

3.1. Vertical covariances

The vertical covariances are represented by multivariate EOFs of surface elevation and vertical profiles of temperature and salinity (Dobricic et al., 2005). Therefore, in each evaluation of the cost function the control vector \mathbf{v} contains coefficients which multiply vertical multivariate EOFs, which are then transformed into corrections of temperature, salinity velocity and surface elevation. The vertical transformation operator \mathbf{V}_V has the form:

$$\mathbf{V}_V = \mathbf{S} \mathbf{\Lambda}^{1/2}, \quad (8)$$

where columns of \mathbf{S} contain multivariate eigenvectors and $\mathbf{\Lambda}$ is a diagonal matrix with eigenvalues of EOFs.

It is important to note in Eq. (7) that we first convert from EOF space into physical space, and then model the horizontal covariances. This means that the three-dimensional spatial covariances \mathbf{V}_S are computed by the multiplication:

$$\mathbf{V}_S = \mathbf{V}_H \mathbf{V}_V. \quad (9)$$

A computationally more efficient approach would be first to apply horizontal covariances in EOF space and then transform the result into physical space: that is, to use the formula:

$$\mathbf{V}_S^* = \mathbf{V}_V \mathbf{V}_H. \quad (10)$$

In Eq. (9) the computational time for the calculation of horizontal covariances is roughly proportional to the product of the number of vertical levels and the number of state vector variables, whilst in Eq. (10) it is proportional to the relatively small number of EOFs. It is clear from Eq. (4) that both approaches result in a matrix \mathbf{B} which is positive definite and symmetric, but they would give the same \mathbf{B} only when vertical EOFs do not vary spatially within the horizontal correlation scales. However, our EOFs vary geographically in 13 regions in the Mediterranean

(Dobricic et al., 2005). In this case the two approaches give very different results at the edges of regions: in Eq. (9) corrections at the edges of regions are discontinuous in EOF space and continuous in physical space, while in Eq. (10) they are continuous in EOF space and discontinuous in physical space. Fig. 1 shows that the application of Eqs. (9) and (10) gives different corrections when EOFs vary within the horizontal correlation scales. It is evident that if we want to produce corrections which are continuous in the physical space, we must apply the computationally more expensive method in Eq. (9).

3.2. Horizontal covariances

It is assumed that horizontal covariances are Gaussian with the constant correlation radius. In oceanographic models, isotropic and Gaussian spatial correlations can be relatively efficiently modelled by a repeated application of the Laplacian operator which is also the solution of the horizontal diffusion equation (e.g. Derber and Rosati, 1989). The application of the Laplacian operator reduces the computational cost by eliminating the explicit calculation of the exponential function between each pair of points and may facilitate the introduction of coastal boundaries. Weaver and Courtier (2001) investigated the application of the diffusion equation to calculate horizontal covariances in the ocean in the presence of coastal boundaries and spherical co-ordinates. However, although much more computationally efficient than the direct application of Gaussian correlation functions, the approximation using the explicit solution of the diffusion equation typically requires a relatively large number of iterations. An alternative to the Laplacian operator is the recursive filter (Lor-

enc, 1992; Hayden and Purser, 1995). It is conceptually simple, typically requires only a few iterations in order to approximate the Gaussian function, and its application on a horizontal grid can be split into two independent directions (Purser et al., 2003). However, in the ocean the application of the recursive filter is more complicated than in the atmosphere, due to the presence of coastlines. Horizontal covariances can be calculated by the recursive filter as a product of following operators:

$$\mathbf{V}_H = \mathbf{W}_y \mathbf{G}_y \mathbf{W}_x \mathbf{G}_x, \quad (11)$$

where \mathbf{G}_x and \mathbf{G}_y represent the recursive filter operators in directions x and y , whilst \mathbf{W}_x and \mathbf{W}_y are diagonal matrices with normalization coefficients which may account for variable grid resolutions in x and y directions. The formulation of normalization matrices \mathbf{W}_x and \mathbf{W}_y , and the implementation of coastal boundary conditions are described below.

3.2.1. Horizontal co-ordinate systems

Oceanographic models often use spherical co-ordinate grids. In this case the distance between points in the longitudinal direction is a function of latitude. To deal with the variable horizontal resolution it is necessary to calculate coefficients of the recursive filter for each model point on the horizontal grid and it is necessary to rescale the filtered field by a spatially varying normalization factor (Weaver and Courtier, 2001; Purser et al., 2003). Practically this factor can be estimated as the inverse of a filtered delta function field defined separately for each model point. On a grid with many ocean points this method can be computationally very expensive, because it requires one application of the filter for each point on the horizontal grid. The

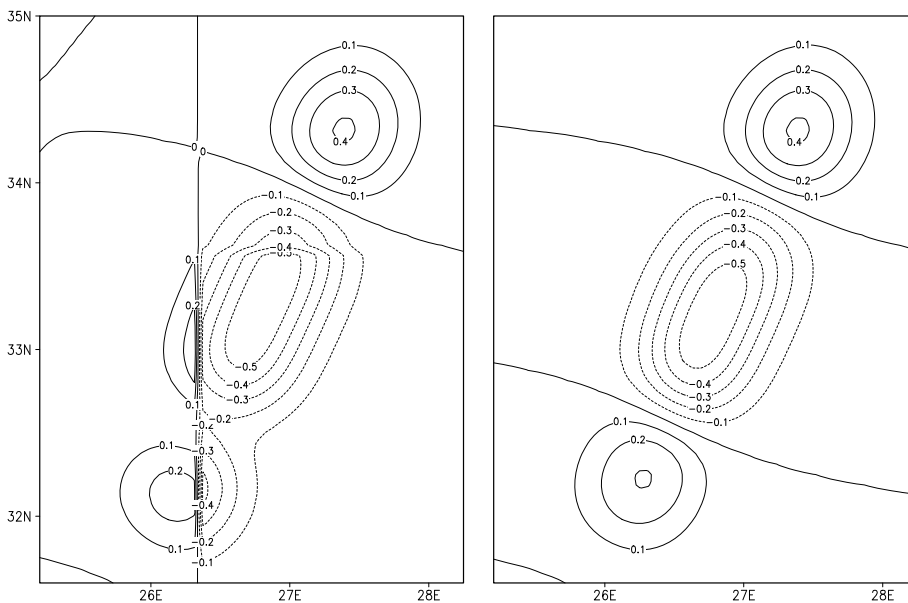


Fig. 1. The impact of the order of the multiplication of vertical and horizontal error covariance operators on typical corrections of the temperature at the first model level ($^{\circ}\text{C}$) along a satellite track which measured SLA. The track crossed four regions with different vertical EOFs, divided by lines which are along the longitude 26.3°E and latitude 33.6°N . In the left panel correlations are obtained by the application of Eq. (10), and in the right panel they are obtained by the application of Eq. (9).

calculation has to be performed once for each model grid set-up and for each choice for the horizontal correlation radius. Weaver and Courtier (2001) propose the randomization of the normalization matrix in order to approximate it in a numerically more efficient way. On the other hand Purser et al. (2003) approximate this factor on a grid with a smoothly varying horizontal resolution by a Taylor expansion of the exact parameters.

In our 3D-VAR we approximate the exact normalization factor by initially forming a look-up table for a relatively small discrete number of grid distances which span resolutions between the minimum and the maximum distance on the grid. The look-up table can be formed by applying the filter only in one direction for each discrete value of the horizontal resolution. Therefore, this preliminary calculation at the initialization phase of the 3D-VAR requires a negligible amount of computational time. Then the normalization factor on each grid point is approximated by interpolating from discrete values in the look-up table either by linear or quadratic interpolation. Fig. 2 shows the impact of the normalization at 40°N. We can see that on a latitude–longitude grid the application of the look-up table practically eliminates the distortion of the shape of the horizontal correction. This solution by look-up table is relatively easy to implement on grids which change the horizontal resolution smoothly. It is important to note that the accuracy of the approximation of the exact isotropic form of the horizontal error correlations is probably not a major problem in modelling the background error covariance matrix. For example, there is much less certainty in estimating background error covariances between different model variables, or even in estimating the horizontal radius of correlation. In comparison to other errors, our solution will be sufficiently accurate if the model grid resolution in the direction of the application of the recursive filter does not vary significantly over several distances of the horizontal correlation radius.

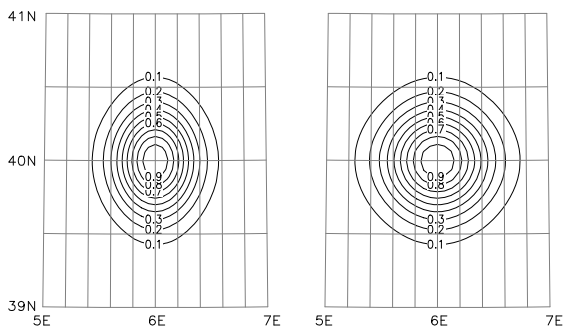


Fig. 2. The impact of the normalization of the recursive filter solution in order to account for the variable horizontal resolution of the model grid. The covariances correspond to a unit perturbation of sea level height (in units of distance) centred at (6°E, 40°N): without the normalization due to the variable horizontal resolution (left), and with the normalization (right). Plots use the Lambert projection. Isolines are plotted with an interval of 0.1 units. The horizontal radius of correlation is set to 30 km, and there are eight iterations by the filter (four by the operator V_H and four by its transpose).

3.2.2. Coastlines

The look-up table defined above cannot estimate normalization factors close to coastlines, because these represent discontinuities and non-homogenous horizontal covariances. It is important to note that in the presence of coastlines with a z co-ordinate model the calculation of the normalization factor from a delta function would be computationally extremely expensive, because it would require one application of the filter for each grid point on every model level. In order to account for coastal boundaries in a computationally efficient way, we first apply an accurate boundary condition inside operators G_x and G_y . In each one-dimensional application of the filter the grid is extended over land by adding several imaginary sea points at coastlines (Fig. 3). The number of points is arbitrary. Typically it spans several horizontal correlation radii. Once the grid is sufficiently extended inland it is not necessary to provide any lateral boundary condition, because with the grid extension we extrapolate the solution over land. After the application of the filter the imaginary points are removed. Therefore, if the number of imaginary points is sufficiently large, the recursive filter does not transfer the information across land.

In one dimension this procedure accurately defines the function at the coastal boundary. However, in two dimensions the solution in each direction is obtained on a different grid, because imaginary sea points are eliminated after each one-dimensional application of the filter. As a result the filter does not provide a symmetric solution which is independent of the order of the applications of one-dimensional filters. Therefore, it is necessary to redefine (11) in terms of a symmetric operator. Symmetry with respect to the order of the application of one-dimensional operators can be achieved in several ways. We have arbitrarily decided to apply the following symmetric form:

$$V_H = \frac{1}{2}(W_y G_y W_x G_x + W_x G_x W_y G_y). \quad (12)$$

This solution doubles the number of computations in each application of the horizontal filter, but it still allows us to apply the recursive filter separately in each direction. It also permits the use of the approximation from the look-up table close to the boundaries in order to prevent anisotropy. Fig. 4 shows an example of the application of the recursive filter near the coasts using Eq. (12).

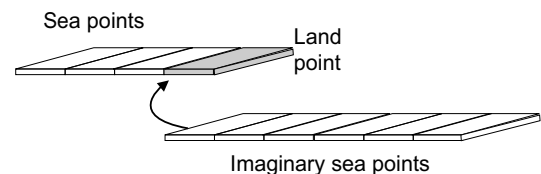


Fig. 3. The insertion of imaginary points at the coasts. Points are inserted at each coastal grid point over the land. The recursive filter is calculated on the extended grid with the larger number of points. After the application of the recursive filter imaginary points are removed.

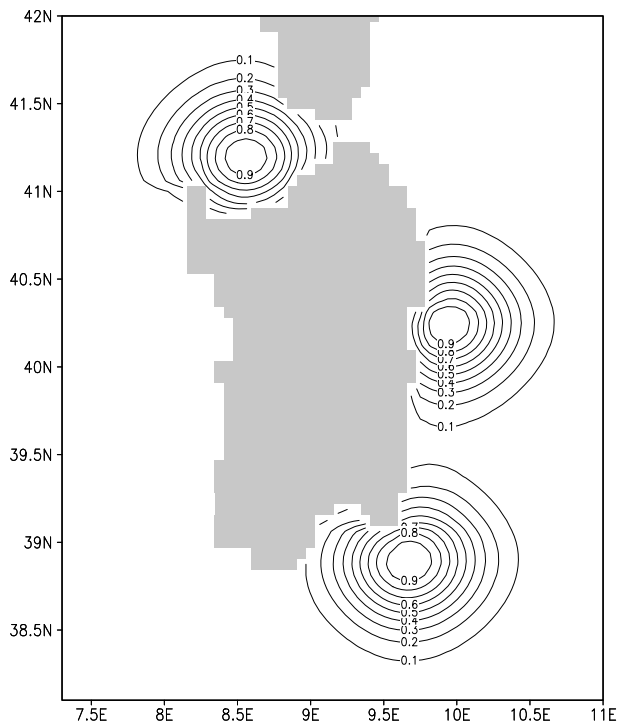


Fig. 4. The filtering result for covariances of sea level height (in units of distance) corresponding to 1.0 unit perturbations in three points close to the coast of Sardinia (Western Mediterranean). The contour interval is 0.1 units. The map projection is stretched latitude–longitude. The correlation radius is 30 km, and eight iterations of the recursive filter were used (four by the operator V_H and four by its transpose). Land points are shaded gray.

An important difference between our solution and the diffusion filter is that the diffusion filter applies the zero gradient boundary condition at coasts (e.g. Weaver and Courtier, 2001), while our solution extrapolates the Gaussian shape of the correlation function. In the absence of any specific information about the correlation structure, we wanted to maintain the approximate Gaussian shape even close to the coast. However, background error covariances close to coasts can be non-isotropic, because dynamical fields there obey kinematic and diffusive boundary conditions (e.g. De Mey, 1997). We assume that, even if we neglect the non-isotropic components of the covariances, during the sequential application of the model integration and the 3D-VAR analysis the background field is corrected frequently enough for the model dynamics to spread the information correctly around the observation. For example, if there is a coastal current, the horizontal advection will soon elongate the correction which initially had an isotropic Gaussian shape along the coast.

Instead of adding imaginary sea points at coastlines, we could estimate the boundary values by a formula with a high-order accuracy. For example, we could use the second-order accurate boundary condition proposed by Hayden and Purser (1995). However, our first tests showed that this second-order boundary condition was producing noisy results when the coastline was complex and observations

were located close to the coast. Furthermore, the application of high-order boundary conditions close to a complex coastline can be technically very difficult. The grid extension by imaginary sea points over land has been chosen because its implementation is technically simple, and it provides an accurate boundary condition even with complex coastlines. These advantages are obtained at the cost of less computational efficiency. However, the grid extension procedure is coded in a way to eliminate a considerable number of land points from the extended grid, and the overall increase of the computational time for the recursive filter operator in realistic applications in the Mediterranean was always less than 30%.

3.3. Free surface operator

The dynamical balance between surface elevation perturbations and the corresponding temperature and salinity perturbations may be estimated either statistically (e.g. Dobricic et al., 2005), or by applying some kind of the geostrophic constraint (e.g. Dobricic et al., 2007). Dobricic et al. (2007) found that the vertical EOF computed solely from the covariance between temperature, salinity and sea level could produce sea level corrections that are not geostrophically balanced with the density corrections. Clearly, if we assimilate only in situ observations of temperature and salinity, the accurate estimation of the corresponding sea level corrections is not an important issue. In that case all unbalanced corrections will be rapidly removed by the fast barotropic adjustment. On the other hand, it was demonstrated in Dobricic et al. (2007) that, when SLA observations were assimilated, the enforcement of the geostrophic relationship for the sea level in the error covariance matrix had a significant positive impact on the accuracy of the analyses. However, the geostrophic relationship is usually assumed with some arbitrary hypothesis on the level of no motion or the bottom pressure gradients. For example, Cooper and Haines (1996) assume that the perturbation bottom pressure gradient is zero, and form the surface elevation perturbation from the vertical integral of temperature and salinity perturbation in the whole water column. Dobricic et al. (2007) use the formula by Pinardi et al. (1995), which assumes that the horizontal pressure gradient at the depth of 1000 m is equal to zero. However, in areas of highly variable bottom topography the assumption of a uniform level of no motion may be wrong, and the correction of the sea level should be derived with more accuracy. The 3D-VAR assimilation system allows the application of complex linear operators which can account for the variability of the bottom topography.

Therefore, we have constructed the operator V_η which gives the steady state results of a barotropic model forced by density perturbations induced by the insertion of temperature and salinity perturbations. The barotropic model equations, discretized in time by the semi-implicit scheme (Kwizak and Robert, 1971), are:

$$\frac{U^{n+1} - U^{n-1}}{\Delta t} - fV^n = -gH \frac{\partial \eta^*}{\partial x} - \int_{-H}^0 \left[\int_{-z}^0 \frac{\partial(\delta b)}{\partial x} dz' \right] dz + \gamma \nabla^2 U^{n-1}, \quad (13)$$

$$\frac{V^{n+1} - V^{n-1}}{\Delta t} + fU^n = -gH \frac{\partial \eta^*}{\partial y} - \int_{-H}^0 \left[\int_{-z}^0 \frac{\partial(\delta b)}{\partial y} dz' \right] dz + \gamma \nabla^2 V^{n-1}, \quad (14)$$

$$\frac{\eta^{n+1} - \eta^{n-1}}{\Delta t} + \left(\frac{\partial U^*}{\partial x} + \frac{\partial V^*}{\partial y} \right) = 0, \quad (15)$$

where U and V are vertically integrated velocity components, f is the Coriolis parameter, g acceleration due to gravity, H the bottom depth, η the surface elevation, $\delta b = g(\delta\rho/\rho_0)$ the buoyancy anomaly, and γ is the coefficient of horizontal viscosity. Horizontal viscosity terms are added in order to speed-up the adjustment. The density perturbation $\delta\rho$ which forces Eqs. (13)–(15) is estimated by the linear equation:

$$\delta\rho = \alpha\delta T - \beta\delta S, \quad (16)$$

where α and β are expansion coefficients for temperature and salinity. Model equations are discretized spatially using the fully staggered C grid. The non-linear advection terms and the bottom friction are neglected, because in the first tests they appeared to be insignificant. The superscripts indicate the time step relative to n , and the superscript “*” indicates the weighted average between two time steps:

$$A^* = aA^{n+1} + (1-a)A^{n-1}, \quad (17)$$

where $0.5 \leq a \leq 1$ in order to have numerically stable solutions (Durran and Klemp, 1983). The choice $a = 0.5$ gives the trapezoidal scheme, and the choice $a = 1$ gives the backwards Euler scheme for the temporal differentiation. Coriolis terms are solved by the leapfrog scheme, and horizontal viscosity terms by the forward Euler scheme. Numerically, Eqs. (13)–(15) are solved by forming an elliptic equation for η^{n+1} which is solved by successive corrections, and then by substituting the solution for η^{n+1} into Eqs. (13) and (14). In Eq. (17) higher values for a filter more the short gravity waves and provide a faster convergence to the steady state. However, initial tests of the model showed that sometimes for $a = 1$ the steady state solution was significantly different to the solution obtained with $a = 0.5$. Therefore, as a compromise between the efficiency and accuracy, the model uses $a = 0.8$. This choice provides a steady state solution which is practically identical to the solution with $a = 0.5$, and converges relatively rapidly (not shown). It was found that the stationary solution is obtained as a daily average already after only a few days of the integration of Eqs. (13)–(15). Expansion coefficients α and β in Eq. (16) are assumed to be constant and

are estimated in advance as mean coefficients calculated from background fields of temperature and salinity. They can also be obtained as a mean of non-linear expansion coefficients calculated on each model grid point during the background run of the ocean model. However, it was found that increasing the level of the accuracy of estimates for α and β had a practically negligible effect on the accuracy of the sea-level perturbation estimate from Eqs. (13)–(15).

After forming corrections in temperature and salinity, we can use the barotropic model to estimate the corrections in sea level. Fig. 5 shows corrections corresponding to temperature and salinity observations by an Argo float for the case with and without the barotropic model. The latter affects the solution in a smaller region than the previous method by Dobricic et al. (2007) and with smaller amplitude.

3.4. Velocity operator

The \mathbf{V}_{uv} operator calculates the velocity corrections by splitting the velocity field into the barotropic and baroclinic components. The barotropic velocity correction is obtained by solving Eqs. (13)–(15), whilst the baroclinic parts of the velocity components u_{bc} and v_{bc} are estimated from the usual dynamic height formula, assuming geostrophic balance:

$$\begin{aligned} f v_{bc} &= \int_{-z}^0 \frac{\partial(\delta b)}{\partial x} dz - \frac{1}{H} \int_{-H}^0 \left[\int_{-z}^0 \frac{\partial(\delta b)}{\partial x} dz' \right] dz, \\ f u_{bc} &= - \int_{-z}^0 \frac{\partial(\delta b)}{\partial y} dz + \frac{1}{H} \int_{-H}^0 \left[\int_{-z}^0 \frac{\partial(\delta b)}{\partial y} dz' \right] dz, \end{aligned} \quad (18)$$

The advantage of the geostrophic assumption is that it requires only a small computational effort, but the disadvantage is that it is not valid at the Equator and may produce velocity vectors orthogonal to the coast. In this study the evaluation of the scheme is made in the Mediterranean, and the geostrophic assumption is valid in the whole model domain. However, in the future it is planned to apply the scheme in a global model set-up, and the baroclinic velocity operator will be substituted by a more general solution which takes into account the equatorial dynamics. Thus our full velocity field corrections are non-geostrophic for the barotropic component and geostrophic for the baroclinic one.

3.5. Divergence damping operator

In the absence of coastlines the velocity operator \mathbf{V}_{uv} imposes a dynamical balance between corrections in velocity, sea surface height and mass fields. The velocity field has only the rotational part for the baroclinic component. However, we need to enforce the zero boundary condition for the total velocity component perpendicular to the coast. As a result, the baroclinic velocity component perpendicular to the coast can suddenly change from its geostrophic value to zero, and the divergence component of the velocity

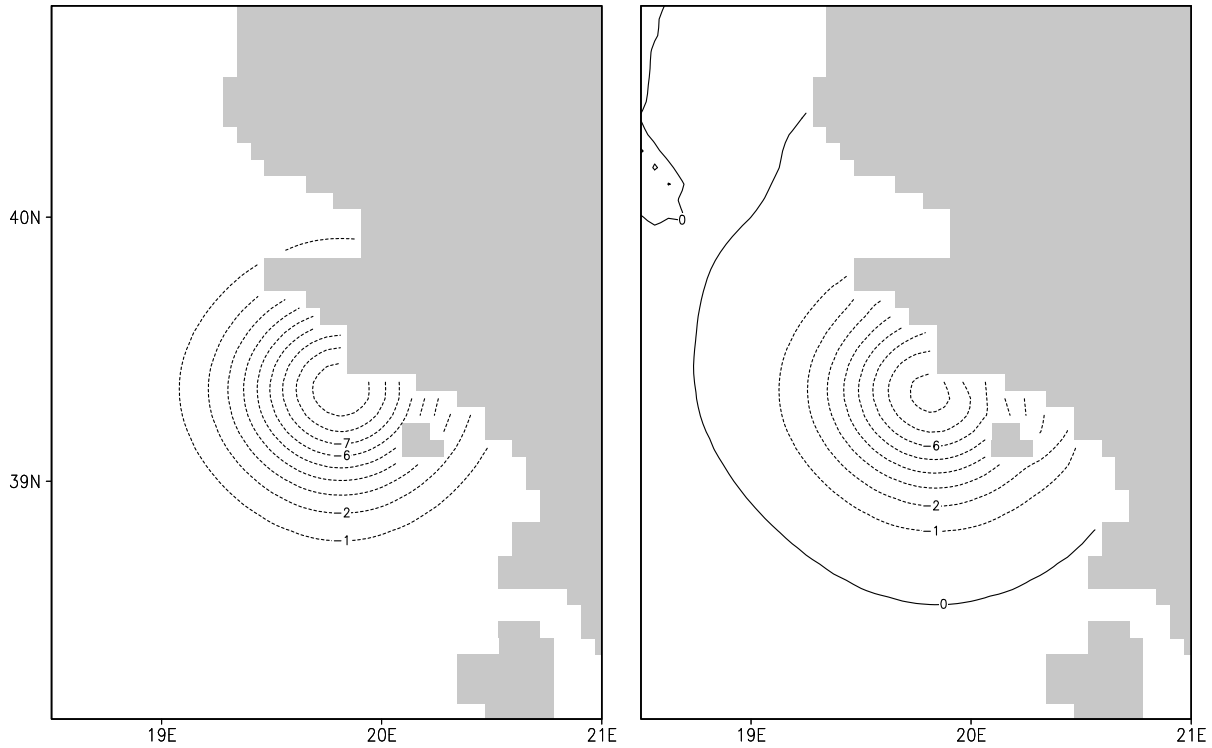


Fig. 5. Impact of the application of the sea surface height operator to the estimate of sea level correction (cm) in a case of an Argo temperature and salinity profile close to the coast of Greece in the Northern Ionian Sea. Left panel shows correction obtained with EOFs obtained by the method described in Dobricic et al. (2007) and the right panel with the barotropic model described in this study.

field may become unrealistically large. Therefore, the divergence damping operator \mathbf{V}_D in (7) will damp velocity divergence near coasts. It filters the divergence part of the velocity field, and maintains the vorticity part unchanged. The filter was successfully applied in the ocean on corrections of velocity close to the coast in order to initialize the analysis (Dobricic et al., 2007). However, it could be especially important to apply the divergence damping operator already inside the 3D-VAR analysis scheme in order to form a more precise estimate of velocity perturbations when assimilating observations close to the coast. The divergence damping is achieved by the successive application of a filter in the form:

$$\delta \mathbf{v}^{n+1} = \delta \mathbf{v}^n + \kappa \nabla D^n, \quad (19)$$

where $\delta \mathbf{v} = (\delta u, \delta v)^T$ is the total velocity increment at each vertical level, superscripts indicate the iteration step number, κ is the filter coefficient, and D is the horizontal divergence of the velocity increments. The effect of the filter is illustrated in Fig. 6. The major impact is at the coastline, where the filter changes the direction of the velocity which initially had an unrealistic direction perpendicular to the boundary. Away from the coast, the impact of the filter is practically negligible. The computational cost of the divergence damping filter is relatively high, because it is applied on each vertical model level. Therefore, this operator is applied only in the last iteration of the outer loop of the numerical minimization. When there are no velocity increments close to the coast the divergence damping operator

practically provides a smoother initial condition for the forecast.

4. Experiments

4.1. Experimental set-up

The 3D-VAR assimilation is applied to the Mediterranean Sea implementation of a general circulation model (Tonani et al., 2008). The model has a free surface which is evolved using an implicit temporal scheme (Madec et al., 1997; Roulet and Madec, 2000). The horizontal resolution is about 7 km in the latitudinal direction and between 6 km and 5 km in the longitudinal direction. The model has 72 levels with a 3 m deep surface layer. Due to the low vertical stratification of the Mediterranean Sea, the first baroclinic Rossby radius of deformation is approximately 10 km (e.g. Robinson et al., 1987). Therefore, the horizontal model resolution of approximately 6 km allows the development of the mesoscale eddies, although the smallest eddies are barely resolved. The atmospheric fluxes of heat and momentum are calculated using interactive bulk formulas. In all experiments heat fluxes are corrected by a term which is proportional to the difference between the model temperature at the surface and daily objective analysis of satellite SST observations (Pinardi et al., 2003). The water flux is estimated by relaxing the surface salinity to monthly climatological values of salinity. A detailed description of the model set-up and the evaluation of its

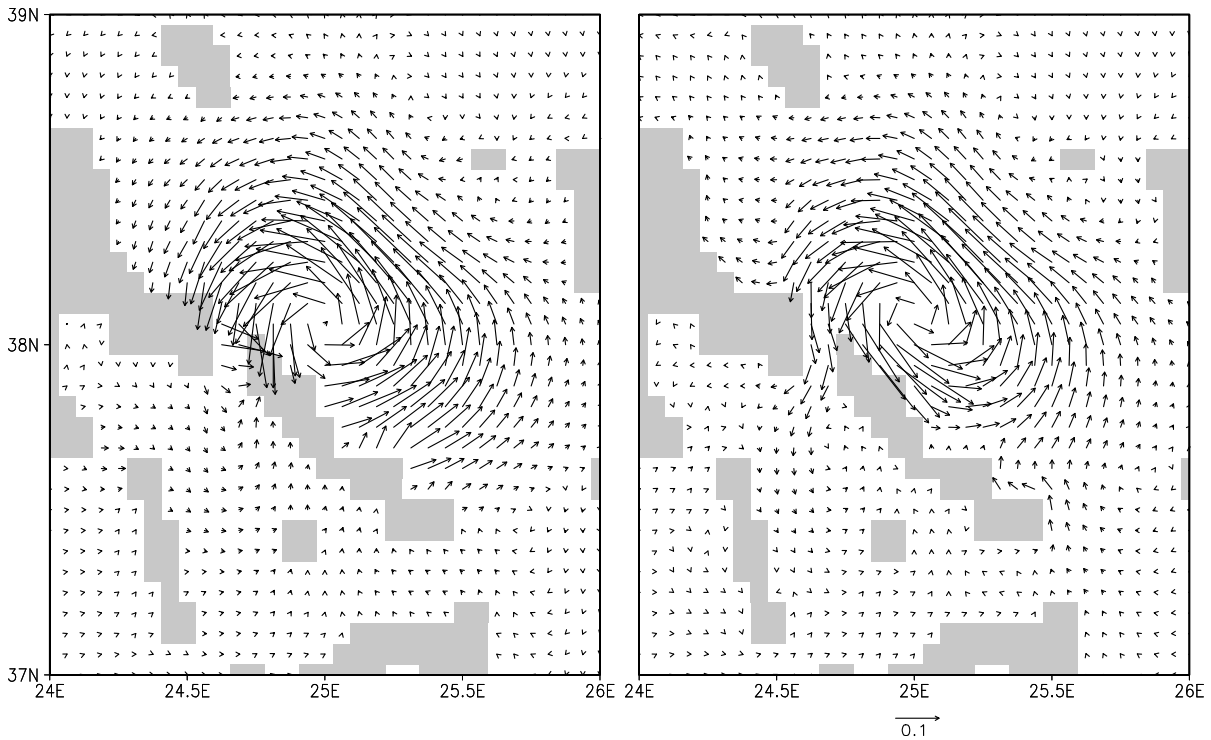


Fig. 6. Impact of the divergence damping operator on corrections of surface velocity (ms^{-1}) corresponding to observations of temperature and salinity profiles by an Argo float in the Aegean Sea (Eastern Mediterranean). The left panel shows corrections produced by the analysis without the application of the divergence damping filter, and the right panel shows filtered corrections. Grid points corresponding to the land are shaded gray.

results are given in Tonani et al. (2008). The size of the model parameter space, which includes sea level, temperature, salinity and velocity defined on the model grid is $\sim 10^8$.

The model bathymetry is shown in Fig. 7. In the Mediterranean Sea the bathymetry has a relatively large variability, with both deep ocean basins, like the Ionian Sea, the Levantine and the Western Mediterranean, and extended and narrow shelves. An interesting area to estimate the global circulation and the exchange between the Eastern and Western Mediterranean is the relatively shallow area of the Strait of Sicily. It has a highly variable bottom topography which is shallower than 1000 m. Relatively shallow areas also cover other regions of the Mediterranean Sea (areas

shaded gray in Fig. 7). In previous implementations of the optimal interpolation scheme the SLA assimilation was carried out only in areas deeper than 1000 m, due to the simple relationship between temperature, salinity and sea level errors (Dobricic et al., 2007). On the other hand, our new application of the barotropic model in the 3D-VAR, gives us the possibility to assimilate observations even in areas with depths lower than 1000 m and highly variable bottom topographies. All experiments started on 10 October 2005 from the operational analysis available on that day. We have assimilated SLA observations along track (Le Traon et al., 2003), XBT profiles (Manzella et al., 2007) and Argo profiles (Poulain et al., 2007). The SLA is assimilated using

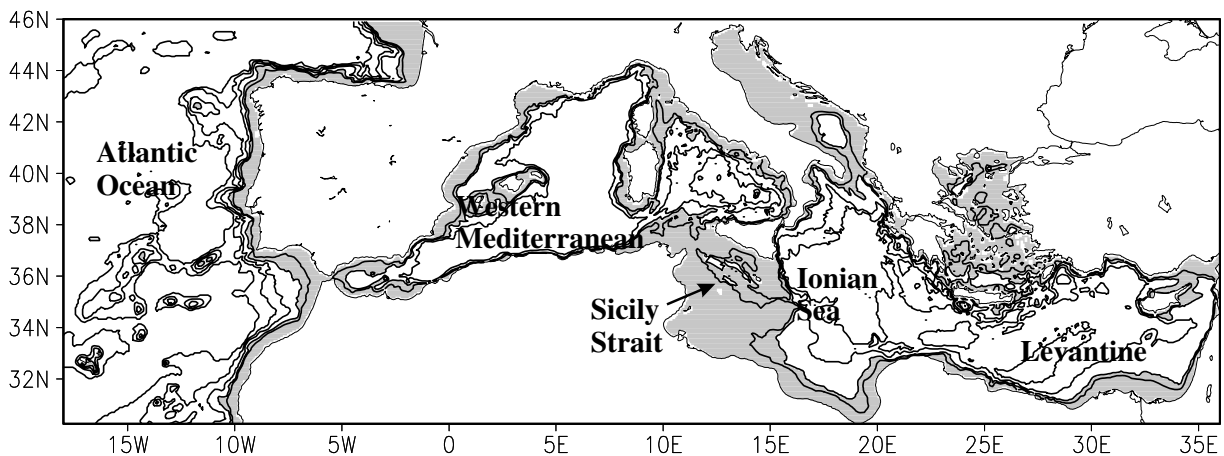


Fig. 7. Model topography. Isolines are plotted at depth of 500 m, 1000 m, 2000 m, 3000 m and 4000 m. Depths above 1000 m are shaded gray.

the mean dynamic topography obtained by correcting the initial estimate by Rio et al. (2007) with un-biased estimates obtained from observations from Argo floats in the period 2003–2005 (Dobricic, 2005).

There are three experiments. The control experiment does not assimilate any observations. In the second experiment all observations are assimilated by the 3D-VAR scheme. Therefore, the comparison between these two experiments shows how much we may improve the accuracy of our estimates of the ocean state by using the 3D-VAR scheme. The third experiment is made with the SOFA scheme using the same set of vertical EOFs as the 3D-VAR but a different construction of the background error covariance. The comparison between the second and the third experiment will show the improvement in the accuracy of the analyses due to the application of a more accurate background error covariance matrix in the 3D-VAR. Both the 3D-VAR and the SOFA schemes assimilate all available observations with the one-day assimilation window.

4.2. Results

The evaluation of the 3D-VAR scheme will be mainly performed by comparing misfits calculated with satellite observations of SLA, and in situ observations of temperature and salinity by Argo floats. It is important to notice that all misfits are calculated before the assimilation of the corresponding observations and therefore the evaluation of the analysis quality is carried out with an independent set of measurements. In this way, we estimate the quality of our analysis by measuring the accuracy of our short term forecasts. Another estimate will be made by calculating the r.m.s. of analysis minus observations. It will show how much our analyses agree with observations. Finally, the sea surface height field at the end of the assimilation period will be qualitatively compared.

Fig. 8a shows the r.m.s. of SLA misfits (the r.m.s. of observations minus background) in the period October 2005–October 2006 for experiments with and without data

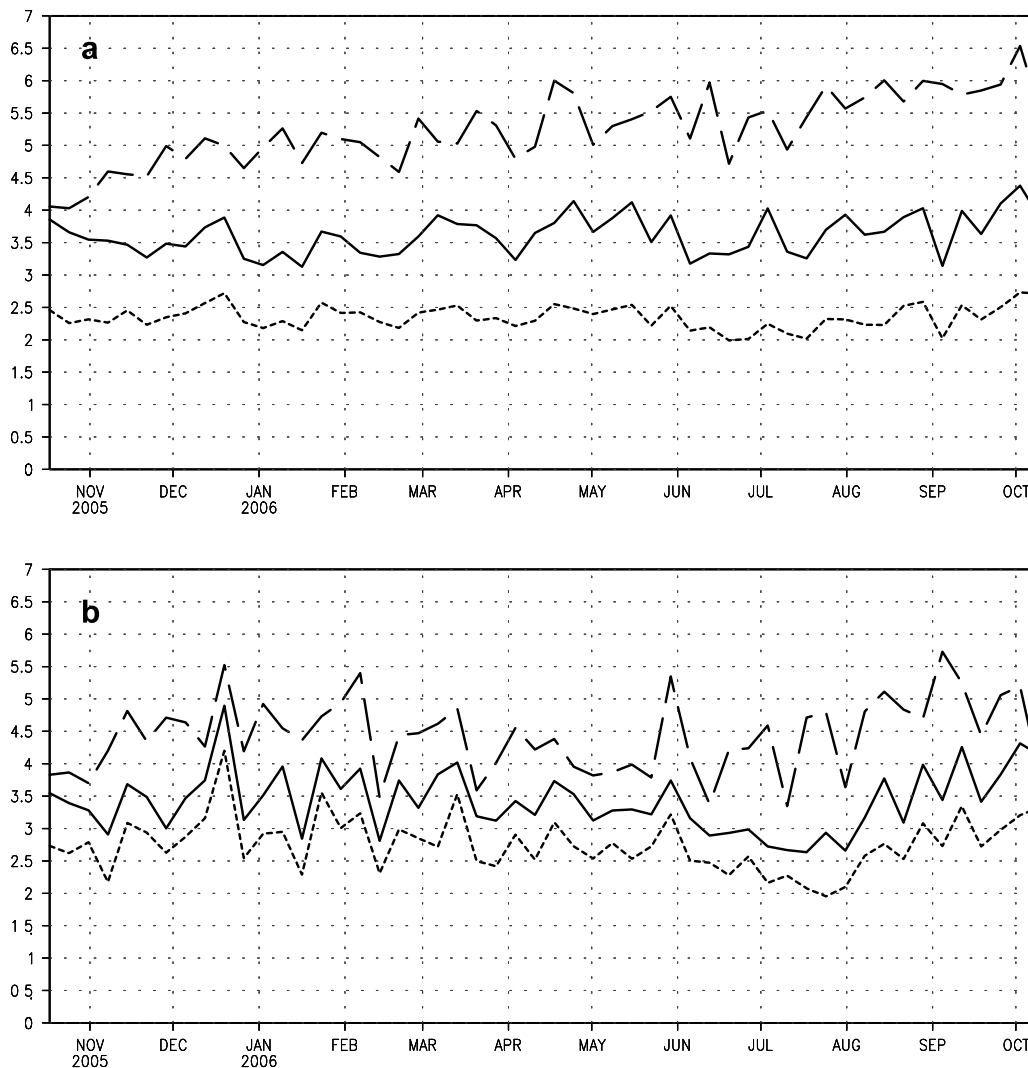


Fig. 8. The weekly r.m.s. of SLA misfits (background-observation) for the experiment with the assimilation by the 3D-VAR (full line), and the experiment without the assimilation (long dashed line), and the r.m.s. of difference between the 3D-VAR analyses and observation (dotted line). All values are in cm. Panel (a) shows results for the whole Mediterranean, and panel (b) only for the Strait of Sicily.

assimilation. We can see in that in the experiment without the data assimilation the r.m.s. of misfits grows with time. After two months it is almost twice the initial r.m.s. of misfits, and it seems that even one year after the start of the experiment it continues to grow, although more slowly. On the other hand, the experiment which assimilates data with the 3D-VAR scheme shows a significantly smaller r.m.s. of misfits, with values that do not show any drift. The figure also shows the r.m.s. of the difference between analysis and observations for the 3D-VAR. We can estimate that the error of SLA observations is 2–3 cm in the open ocean (e.g. Menard et al., 2003), and becomes slightly higher for our data due to corrections for tides, atmospheric pressure and steric effects. Therefore, as a confirmation of the good quality of SLA analyses, we can see in Fig. 8a that the analysis error is on average 2.5 cm, i.e., it is within the SLA observational error. Fig. 8b shows r.m.s. of SLA misfits for the Strait of Sicily. We can see that even in shallow areas the 3D-VAR analyses have smaller

errors than the assimilation run. However, in this case the improvement is smaller. The major reason for the smaller improvement is that the experiment without assimilation already gives smaller r.m.s. misfits than for the whole Mediterranean. Furthermore, the r.m.s. of analysis minus observations is slightly higher than that obtained for the whole Mediterranean, indicating that the background error covariances are somewhat underestimated.

Fig. 9 shows the relative difference between the r.m.s. of background minus observations and analysis minus observations, calculated by the 3D-VAR and SOFA schemes. It is calculated using the formula:

$$r = \frac{D_{\text{VAR}} - D_{\text{OI}}}{D_{\text{VAR}}}, \quad (20)$$

where D_{VAR} is the r.m.s. difference in the 3D-VAR experiment, and D_{OI} is the r.m.s. difference in the SOFA experiment. Initially the two schemes give similar estimates for the whole basin when measured in terms of misfits

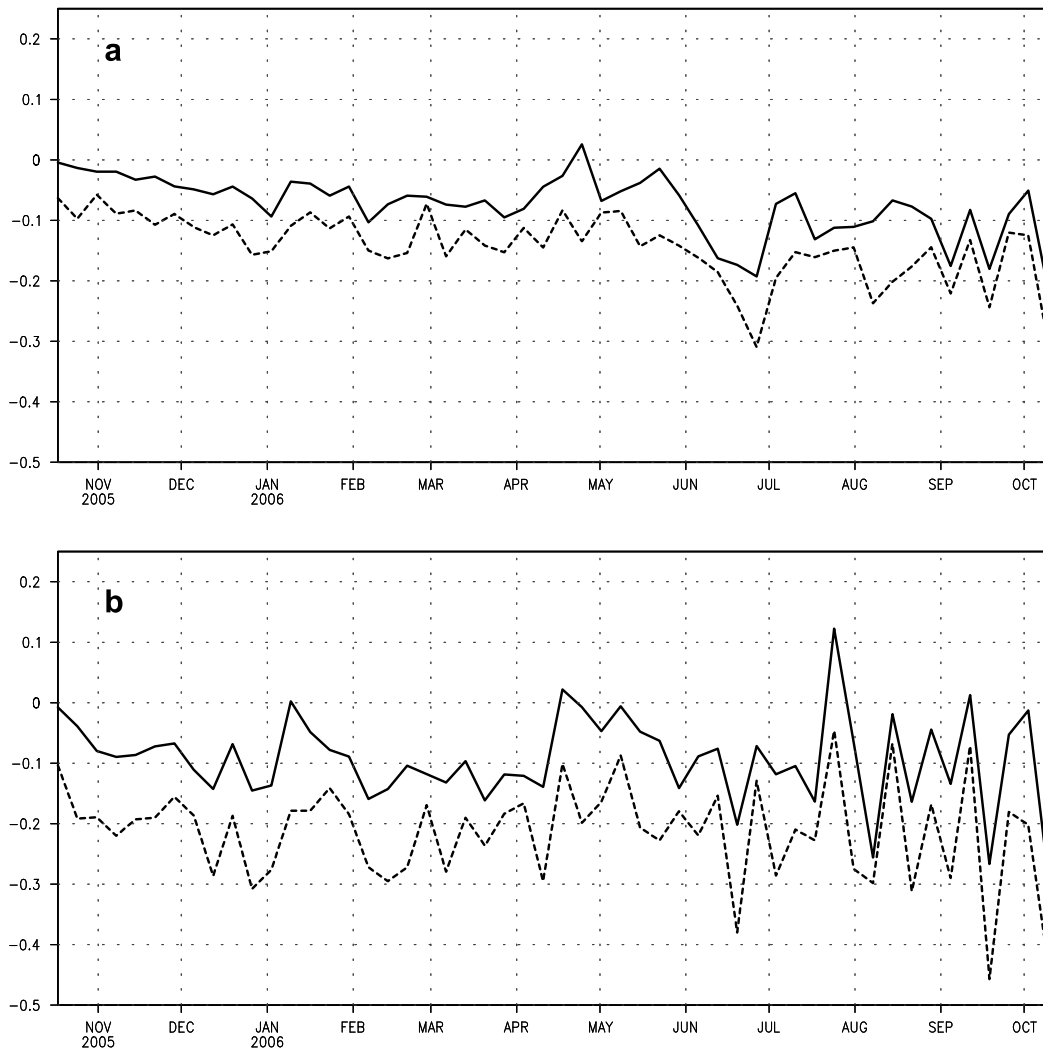


Fig. 9. The full line shows the relative difference between the weekly r.m.s. of SLA misfits (background-observation) for the experiment with the assimilation by the 3D-VAR and the experiment with the assimilation by the SOFA. The dotted line shows the relative difference between the r.m.s. of the difference between analyses and observation for 3D-VAR and SOFA analyses and observations. The expression for the calculation of the relative difference is given by Eq. (20).

(Fig. 9a). On the other hand, the 3D-VAR analysis are 5–10% closer to observations. During the assimilation period the discrepancy between estimates by the two assimilation systems continuously grows. After one year 3D-VAR produces $\sim 10\%$ smaller misfits, whilst the analyses are 15–20% closer to the observations. In the shallow area of the Sicily Strait at the beginning of the assimilation period 3D-VAR already gives $\sim 10\%$ smaller misfits, and the analyses are $\sim 20\%$ closer to observations (Fig. 9b). The same result is maintained throughout the assimilation period. The reason for the differences in the analyses between 3D-VAR and SOFA scheme is that the 3D-VAR scheme assimilates data in shallow areas. Initially, the impact of these observations is significant only locally, but with time it becomes more important on the basin scale.

The left panel in Fig. 10 shows r.m.s. and biases of temperature misfits calculated as Argo observation minus background value. The experiment with 3D-VAR analyses has a lower r.m.s. of misfits than the experiment without assimilation. Furthermore, with the assimilation the bias becomes practically insignificant in deeper layers of the ocean. It is still significant at ~ 50 m depth which approximately corresponds to the bottom of the summer mixed layer. Its negative value indicates that the model systematically overestimates the mixed layer depth in summer. Similarly, the r.m.s. of temperature misfits has the maximum at the bottom of the summer mixed layer.

Both bias and r.m.s. of misfits are relatively small close to the surface, probably due to the fact that in both experiments surface temperature is relaxed towards satellite SST observations. The right panel in Fig. 10 shows the r.m.s. and biases of salinity misfits (observations minus background). The assimilation significantly reduces the bias, especially at depths between 100 m and 300 m. This is the layer of the local salinity maximum in the Eastern Mediterranean in which the Levantine Intermediate Water (LIW) spreads towards the Strait of Sicily and the Western Mediterranean (e.g. Pinardi et al., 2005). Without the assimilation the model systematically underestimates the salinity in LIW. Furthermore, we can also see that the r.m.s. of misfits is significantly reduced with the data assimilation. However, in both experiments the bias and the r.m.s. of misfits increase towards the surface where they reach the maximum value. This behavior can be explained by the fact that in the model the water and salt flux is computed by relaxing the surface salinity towards a climatology (Tonani et al., 2008). Therefore, it seems that the assimilation is not able to correct the drift of the surface salinity towards the climatology which is fresher than observations. When compared to Argo observations the difference in the analyses between the 3D-VAR and the SOFA was insignificant (not shown). Clearly the major improvement of the 3D-VAR scheme with respect to SOFA is in the SLA assimilation, since

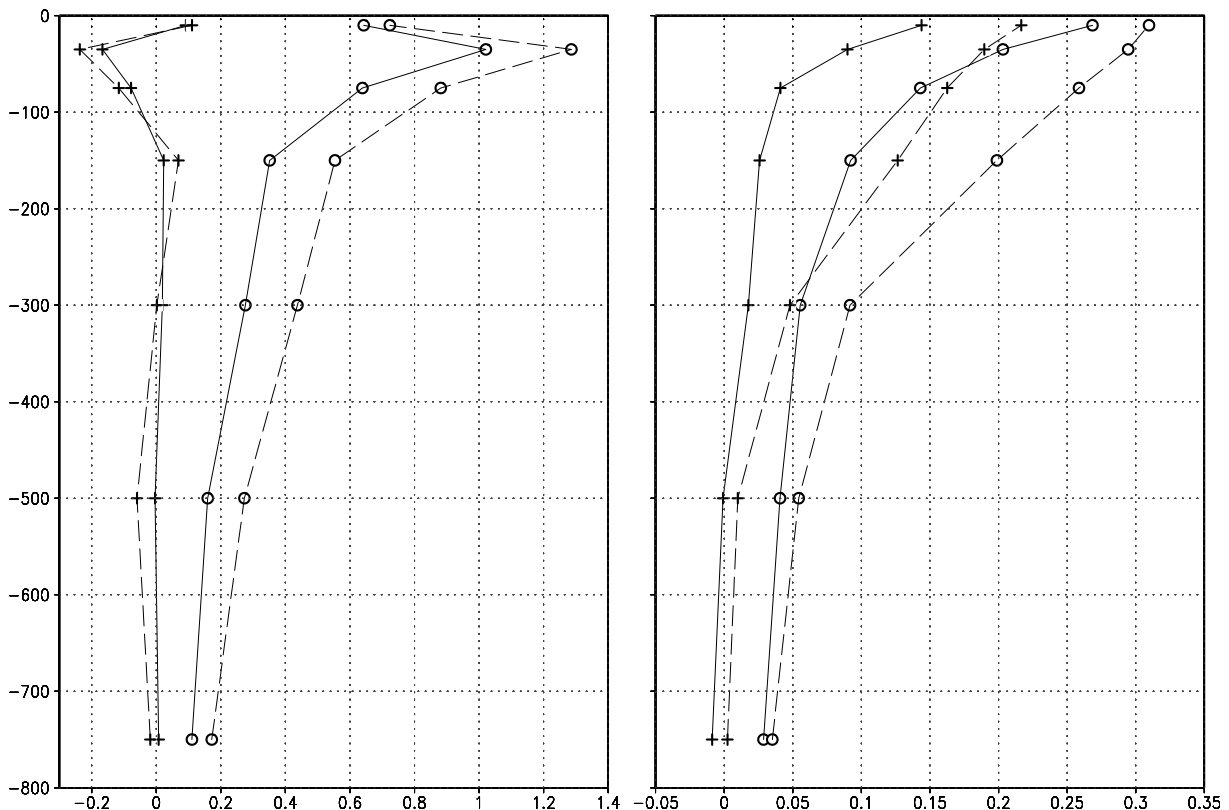


Fig. 10. The r.m.s. and biases of misfits for the year-long period of the 3D-VAR and the simulation experiments. The left panel shows results for the temperature ($^{\circ}\text{C}$), and the right panel for salinity (PSU). Dots indicate the r.m.s. of misfits, and crosses indicate biases. The experiment with the assimilation by the 3D-VAR is indicated by full lines, and the experiment without the assimilation with dashed lines.

it is there that the effects of the bottom topography and the coastline constraints are more important.

To show how the assimilation impacts the quality of state estimates in the Mediterranean Sea, the sea surface elevation field produced by the three experiments is displayed in Fig. 12. The major differences between the simulation and the 3D-VAR are in the position and intensity of

several eddies like the Iera-Petra eddy (centred at 26°E and 34°N), the Pelops eddy (centred at 21°E and 36°N) and the meandering of the Atlantic Ionian Stream (AIS) in the Northern Ionian Sea (the gradient between high and low areas between 35°N and 36°N). Both the Iera-Petra and Pelops eddies were present in the initial analysis in October 2005 (not shown). After one year in the experiment without

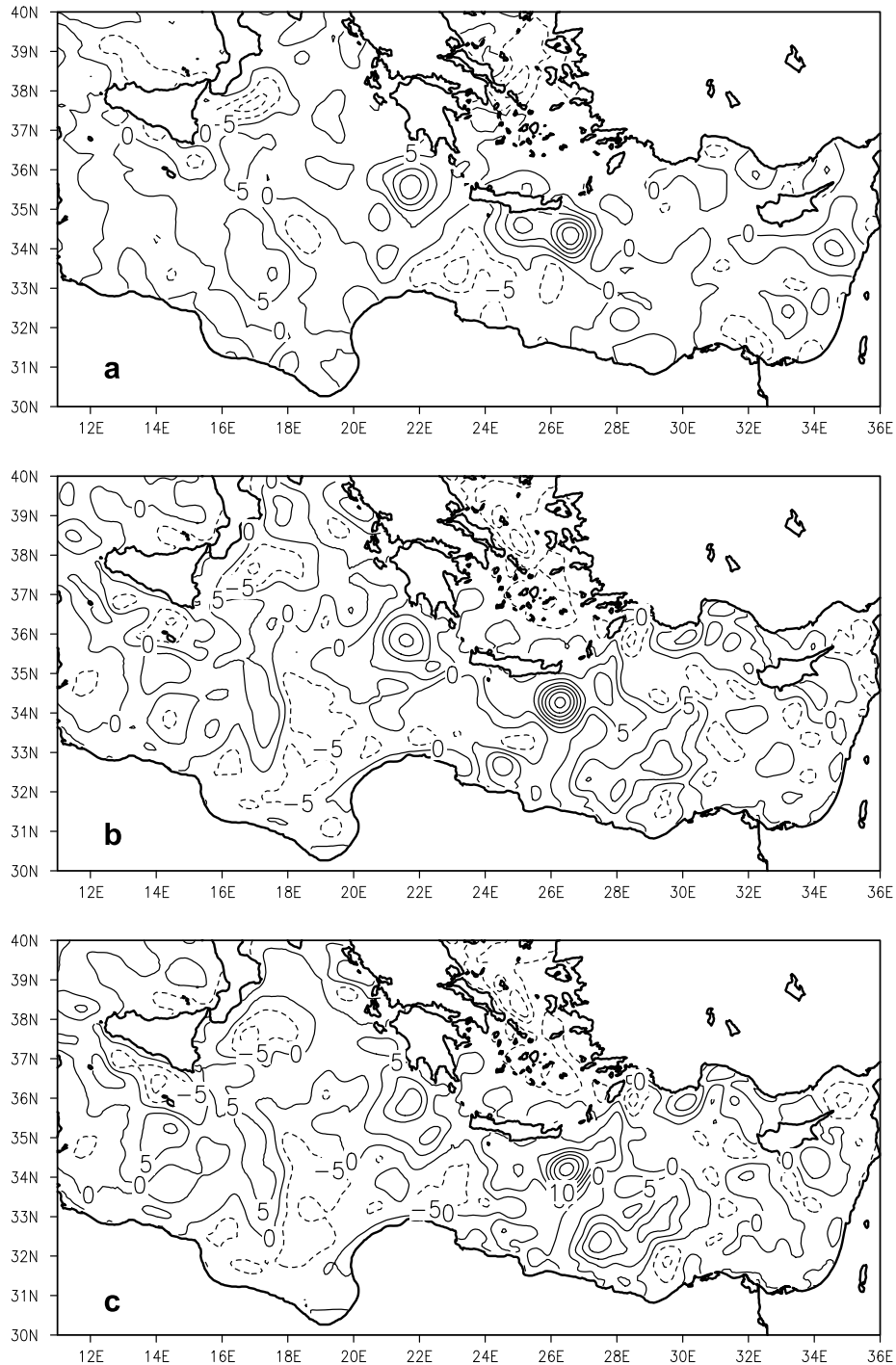


Fig. 11. Comparison between SLA fields (cm): (a) AVISO objective analysis for SLA in the week from 11 October 2006 to 17 October 2006, (b) the 3D-VAR estimate on 15 October 2006, and (c) the SOFA estimate on 15 October 2006. The mean SLA over the area is subtracted from each field in order to eliminate from the comparison the influence of the steric height and basin scale barotropic effects.

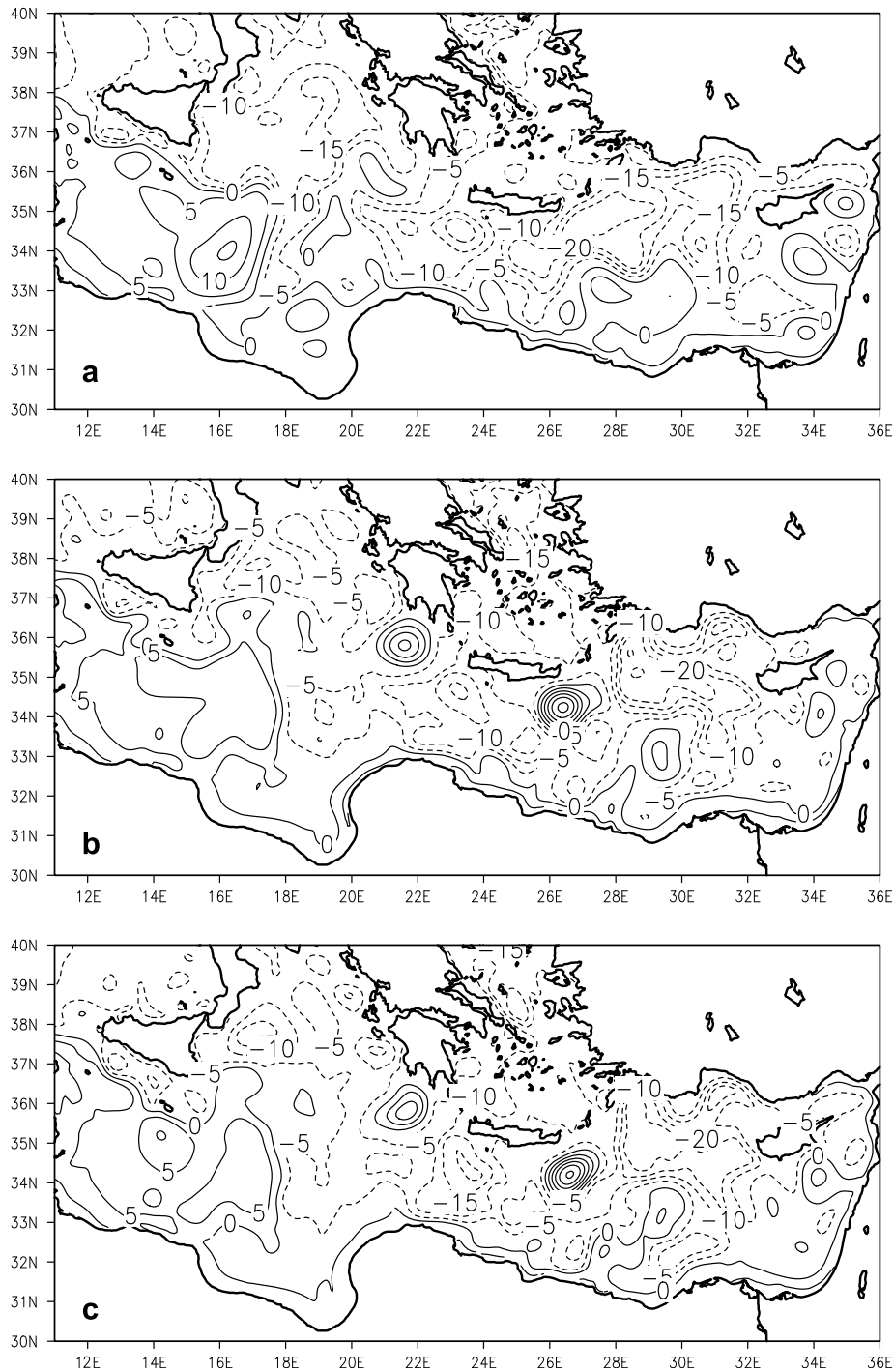


Fig. 12. Comparison between sea level fields (cm) obtained on 15 October 2006: (a) the experiment without the assimilation, (b) the experiment with the assimilation by 3D-VAR, and (c) experiment with the assimilation by SOFA.

data assimilation the Pelops eddy almost disappeared, and instead of the anticyclonic Iera-Petra eddy there is a uniform cyclonic circulation covering the whole northern Levantine. On the other hand, with the data assimilation both Pelops and Iera-Petra are strong anticyclonic eddies which dominate large areas of the surface circulation in the Levantine. Furthermore, the experiment started with the AIS which was directed straight across the Ionian Sea (not shown). After one year without data assimilation the AIS

did not change the initial direction significantly, and the circulation in the Northern Ionian Sea is mainly cyclonic. With the data assimilation the AIS changes the initial direction and meanders into the Northern Ionian Sea, as has often been observed (e.g. Pinardi et al., 2005). The comparison between the analysis obtained by the 3D-VAR and the analysis obtained by the SOFA scheme (Fig. 12b and c) shows small qualitative differences. The differences in accuracy shown in Fig. 9a are significant only

at small spatial scales. Fig. 11 compares the estimate of the SLA field by the AVISO objective analysis for the week between October 11 and October 17 and the SLA analysis by the 3D-VAR and SOFA schemes for the October 15. Once again, major differences are at small spatial scales, and the differences between 3D-VAR and SOFA have a similar size to the differences between 3D-VAR and objective analyses by the AVISO.

5. Conclusions

The study describes the development and implementation of a new oceanographic 3D-VAR assimilation system. Several new solutions were applied in order to model in a computationally efficient way the background error covariances in the ocean. The horizontal filtering has been developed in a way to eliminate discontinuities due to the regional definition of EOFs. Furthermore, Gaussian horizontal covariances have been modelled with a recursive filter that considers the presence of complex coastal boundaries. Covariances between errors in the sea level and errors in temperature and salinity vertical profiles were estimated using a steady state solution of a barotropic ocean model, which accurately accounts for the variability of the bottom topography. The velocity errors were adjusted along the coasts using the divergence damping filter. All these solutions simplify the application of the 3D-VAR assimilation system in complex areas like the Mediterranean Sea which combine the deep ocean with coastal shelves. The application of vertical EOFs and the use of the recursive filter makes our scheme similar to some meteorological 3D-VAR schemes (Lorenc et al., 2000; Barker et al., 2004), whereas the treatment of coastal boundaries and the application of the barotropic model are specific oceanographic features.

The background error covariances in our 3D-VAR scheme dynamically connect all model state variables. This approach differs from the common practice in the meteorological applications of the 3D-VAR in which some parameters contain uncorrelated and correlated parts (Derber and Bouttier, 1999; Weaver et al., 2005). Our choice was based on a long experience with the SOFA scheme. However, if we want to split temperature and salinity covariances into correlated and uncorrelated parts, it is sufficient to use another set of vertical EOFs, in which some EOFs do not contain covariances between temperature and salinity. Furthermore, the state vector can contain wind stress uncorrelated with vertical EOFs of temperature and salinity. The corrections to the wind stress can be used as the additional forcing term in the barotropic model, in order to account for errors in the sea level that are not correlated with temperature and salinity errors. It should also be noticed that, as our 3D-VAR applies first vertical and then horizontal operators, it is possible to define different horizontal radii of correlation at each horizontal level, using the same solution for horizontal covariances with coastal boundary conditions. However, in that case even

when vertical EOFs do not change in different geographical regions, the vertical and the horizontal modes will no longer be independent.

The 3D-VAR scheme developed in this study represents a software structure which may be improved in the future. For example, a 4D-VAR scheme can be constructed directly from 3D-VAR by adding the tangent linear approximation of the model to the observational operator (e.g. Weaver et al., 2003). However, when the oceanographic model has a high resolution, the linear approximation can be wrong. If it is not possible to linearize the model, the computationally much more demanding Monte Carlo approach may be used to estimate background error covariances (e.g. van Leeuwen, 2003). Some computational savings in the Monte Carlo method may be obtained by reduced space approximations as in the SEEK filter (Brasseur and Verron, 2006). Independently of the form of the background error covariances, one can use the structure of the minimizer, observational operators and their adjoints from the existing 3D-VAR scheme. Furthermore, we can horizontally localize covariances using recursive filters. The update of the background covariance matrix after the analysis may be obtained from the Hessian of the cost function (e.g. Tarantola, 2005).

An important improvement of the 3D-VAR scheme will be to assimilate new types of observation. As the computational time of the 3D-VAR scheme mainly depends on the size of the state vector, it becomes feasible to assimilate large observational sets like satellite observations of sea surface temperature. Another possibility will be to assimilate trajectories of Argo floats or surface drifters. The trajectory assimilation can be achieved by adding a tangent linear model of the trajectory to the observational operator in Eq. (2). These potential advantages of the 3D-VAR scheme should be confirmed during its future applications.

Acknowledgements

The AVISO objective analysis was produced by SSALTO/DUACS and distributed by AVISO, with support from CNES. This work was partially supported by the EU project MERSEA (Contract No. SIP3-CT-2003-502885). We would like to thank the two unknown reviewers for their very useful comments and suggestions. We are grateful to Emanuele di Lorenzo for stimulating discussions.

References

- Barker, D.M., Huang, W., Guo, Y.-R., Bourgeois, A.J., Xiao, Q.N., 2004. A three-dimensional variational data assimilation system for MM5: implementation and initial results. *Monthly Weather Review* 132, 897–914.
- Bellucci, A., Masina, S., Di Pietro, P., Navarra, A., 2008. Using temperature-salinity relations in a global implementation of a multivariate data assimilation scheme. *Monthly Weather Review* 135, 3785–3807.

- Brandt, A., 1977. Multi-level adaptive solutions to boundary value problems. *Mathematics of Computation* 31, 333–390.
- Brasseur, P., Bahurel, P., Bertino, L., Birol, F., Brankart, J.-M., Ferry, N., Losa, S., Remy, E., Schröter, J., Skachko, S., Testut, C.-E., Tranchant, B., van Leeuwen, P.-J., Verron, J., 2005. Data assimilation for marine monitoring and prediction: the MERCATOR operational assimilation systems and the MERSEA developments. *Quarterly Journal of the Royal Meteorological Society* 131, 3561–3582.
- Brasseur, P., Verron, J., 2006. The SEEK filter method for data assimilation in oceanography: a synthesis. *Ocean Dynamics* 56, 650–661.
- Briggs, W.L., Henson, V.E., McCormick, S.F., 2000. *A Multigrid Tutorial*, second ed. SIAM, Philadelphia, USA.
- Byrd, R.H., Lu, P., Nocedal, J., Zhu, C., 1995. A limited memory algorithm for bound constrained optimization. *SIAM Journal on Scientific Computing* 16, 1190–1208.
- Cooper, M., Haines, K., 1996. Data assimilation with water property conservation. *Journal of Geophysical Research* 101, 107–1059.
- Courtier, P., Thepaut, J.-N., Hollingsworth, A., 1994. A strategy for operational implementation of 4D-VAR using an incremental approach. *Quarterly Journal of the Royal Meteorological Society* 123, 2449–2461.
- De Mey, P., 1997. Data assimilation at the oceanic mesoscale: a review. *Journal of the Meteorological Society of Japan* 75, 281–306.
- De Mey, P., Benkiran, M., 2002. A multivariate reduced-order optimal interpolation method and its application to the Mediterranean basin-scale circulation. In: Pinardi, N., Woods, J. (Eds.), *Ocean Forecasting*. Springer Verlag, pp. 281–306.
- Demirov, E., Pinardi, N., Fratianni, C., Tonani, M., Giacomelli, L., De Mey, P., 2003. Assimilation scheme in the Mediterranean forecasting system: operational implementation. *Annales Geophysicae* 21, 189–204.
- Derber, J., Rosati, A., 1989. A global oceanic data assimilation system. *Journal of Physical Oceanography* 19, 1333–1347.
- Derber, J., Bouttier, F., 1999. A reformulation of the background error covariance in the ECMWF global data assimilation system. *Tellus* 51A, 195–222.
- Dobricic, S., 2005. New mean dynamic topography of the Mediterranean calculated from assimilation system diagnostics. *Geophysical Research Letters* 32, 11606.
- Dobricic, S., Pinardi, N., Adani, M., Bonazzi, A., Fratianni, C., Tonani, M., 2005. Mediterranean forecasting system: an improved assimilation scheme for sea-level anomaly and its validation. *Quarterly Journal of the Royal Meteorological Society* 131, 3627–3642.
- Dobricic, S., Pinardi, N., Adani, M., Tonani, M., Fratianni, C., Bonazzi, A., Fernandez, V., 2007. Daily oceanographic analyses by the Mediterranean basin scale assimilation system. *Ocean Sciences* 3, 149–157.
- Durran, D.R., Klemp, J.B., 1983. A compressible model for the simulation of moist mountain waves. *Monthly Weather Review* 111, 2341–2361.
- Fujii, Y., Kamachi, M., 2003. Three-dimensional analysis of temperature and salinity in the equatorial Pacific using a variational method with vertical coupled temperature–salinity empirical orthogonal function modes. *Journal of Geophysical Research* 108, 3217. doi:10.1029/2002JC001745.
- Gauthier, P., Charete, C., Filion, L., Koclas, P., Laroche, S., 1999. Implementation of a 3D variational data assimilation system at the Canadian Meteorological Centre. Part I: global analysis. *Atmosphere-Ocean* 37, 103–156.
- Giering, R., Kaminski, T., 1998. Recipes for adjoint code construction. *ACM Transactions on Mathematical Software* 24, 437–474.
- Hayden, C.M., Purser, R.J., 1995. Recursive filter objective analysis of meteorological fields: applications to NESDIS operational processing. *Journal of Applied Meteorology* 34, 3–15.
- Kwizak, M., Robert, A.J., 1971. A semi-implicit scheme for grid point atmospheric models of the primitive equations. *Monthly Weather Review* 99, 32–36.
- Le Traon, P.Y., Nadal, F., Ducet, N., 2003. An improved mapping method of multisatellite altimeter data. *Journal of Atmospheric and Oceanic Technology* 15, 522–533.
- Lorenc, A.C., 1992. Iterative analysis using covariance functions and filters. *Quarterly Journal of the Royal Meteorological Society* 118, 569–591.
- Lorenc, A.C., 1997. Development of an operational variational assimilation scheme. *Journal of the Meteorological Society of Japan* 75, 339–346.
- Lorenc, A.C., Ballard, S.P., Bell, R.S., Ingleby, P.I., Andrews, P.L.F., Barker, D.M., Bray, J.R., Clayton, A.M., Dalby, T., Li, D., Payne, T.J., Saunders, F.W., 2000. The Met. Office global three-dimensional variational data assimilation scheme. *Quarterly Journal of the Royal Meteorological Society* 126, 2991–3012.
- Madec, G., P. Delecluse, M. Imbard, Lévy, C., 1997. OPA version 8. Ocean general circulation model reference manual. Rapp. Int., LODYC, France, 200pp.
- Manzella, G.M.R., Reseghetti, F., Coppini, G., Borghini, M., Cruzado, A., Galli, C., Gertman, I., Gervais, T., Hayes, D., Millot, C., Murashkovsky, A., Ozsoy, E., Tziavos, C., Velasquez, Z., Zodiatis, G., 2007. The improvements of the ships of opportunity program in MFSTEP. *Ocean Sciences* 3, 245–258.
- Masina, S., Pinardi, N., Navarra, A., 2001. A global ocean temperature and altimeter data assimilation system for studies of climate variability. *Climate Dynamics* 17, 687–700.
- Menard, Y., Fu, L.-L., Escudier, P., Parisot, P., Perbos, J., Vincent, P., Desai, S., Haines, B., Kunstmann, G., 2003. The Jason-1 mission. *Marine Geodesy* 26, 131–146.
- Pinardi, N., Rosati, A., Pacanowski, R.C., 1995. The sea surface pressure formulation of rigid lid models. Implications for altimetric data assimilation studies. *Journal of Marine Systems* 6, 109–119.
- Pinardi, N., Allen, I., Demirov, E., De Mey, P., Korres, G., Lascaratos, A., Le Traon, P.Y., Maillard, C., Manzella, G., Tziavos, C., 2003. The Mediterranean ocean forecasting system: first phase of implementation (1998–2001). *Annales Geophysicae* 21, 3–20.
- Pinardi, N., Arneri, E., Crise, A., Ravaioli, M., Zavatarelli, M., 2005. The physical, sedimentary and ecological structure and variability of shelf areas in the Mediterranean Sea. In: Robinson, A.R., Brink, K. (Eds.), *The Sea*, vol. 14. Harvard University Press, Cambridge, USA, pp. 1243–1330.
- Poulain, P.-M., Barbanti, R., Font, J., Cruzado, A., Millot, C., Gertman, I., Griffa, A., Molcard, A., Rupolo, V., Le Bras, S., Petit de la Villeon, L., 2007. MedArgo: a drifting profiler program in the Mediterranean Sea. *Ocean Sciences* 3, 379–395.
- Purser, R.J., Wu, W.-S., Parish, D.F., Roberts, N.M., 2003. Numerical aspects of the application of recursive filters to variational statistical analysis. Part II: spatially inhomogeneous and anisotropic covariances. *Monthly Weather Review* 131, 1524–1535.
- Rabier, F., 2005. Overview of global data assimilation developments in numerical weather-prediction centres. *Quarterly Journal of the Royal Meteorological Society* 131, 3215–3233.
- Rio, M.E., Poulain, P.-M., Pasqual, A., Mauri, E., Larnicol, G., Santoleri, L., 2007. A mean dynamic topography of the Mediterranean Sea computed from the altimetric data and in situ measurements. *Journal of Marine Systems* 65, 484–508.
- Robert, C., Durbiano, S., Blayo, E., Verron, J., Blum, J., Le Dimet, F.-X., 2005. A reduced-order strategy for 4D-Var data assimilation. *Journal of Marine Systems* 57, 70–82.
- Robinson, A.R., Hecht, A., Pinardi, N., Bishop, J., Leslie, W.G., Rosentroub, Z., Mariano, A.J., Brenner, S., 1987. Small synoptic/mesoscale eddies and energetic variability of the eastern Levantine basin. *Nature* 327, 131–134.
- Roulet, G., Madec, G., 2000. Salt conservation, free surface and varying volume: a new formulation for ocean GCMs. *Journal of Geophysical Research* 105, 23927–23942.
- Stammer, D., Wunsch, C., Giering, R., Eckert, C., Heimbach, P., Marotzke, J., Adcroft, A., Hill, C.N., Marshall, J., 2002. Global ocean circulation during 1992–1997, estimated from ocean observa-

- tions and a general circulation model. *Journal of Geophysical Research* 107. doi:10.1029/2001JC000888.
- Tarantola, A., 2005. *Inverse Problem Theory and Methods for Model Parameter Estimation*. SIAM, pp. 342.
- Tonani, M., Pinardi, N., Dobricic, S., Adani, M., Marzocchi, F., 2008. A high resolution free surface model of the Mediterranean Sea. *Ocean Sciences* 4, 1–14.
- van Leeuwen, P.J., 2003. A variance-minimizing filter for large-scale applications. *Monthly Weather Review* 131, 2071–2084.
- Weaver, A.T., Courtier, P., 2001. Correlation modelling on the sphere using a generalized diffusion equation. *Quarterly Journal of the Royal Meteorological Society* 127, 1815–1846.
- Weaver, A.T., Vialard, J., Anderson, D.L.T., 2003. Three- and four-dimensional variational assimilation with an ocean general circulation model of the tropical Pacific Ocean. Part 1: formulation, internal diagnostics and consistency checks. *Monthly Weather Review* 131, 1360–1378.
- Weaver, A.T., Deltel, C., Machu, E., Ricci, S., Daget, N., 2005. A multivariate balance operator for variational ocean data assimilation. *Quarterly Journal of the Royal Meteorological Society* 131, 3605–3625.